Research in Astronomy and Astrophysics, 24:065026 (8pp), 2024 June https://doi.org/10.1088/1674-4527/ad484f

Long-term Integration Ability of the Submillimeter Wave Astronomy Satellite (SWAS) Spectral Line Receivers

Bing-Ru Wang[1,2], Di Li[1,3,8], Paul F. Goldsmith[4], Jingwen Wu[2,1,8], Chao-Wei Tsai[1,5], Rudolf Schieder[6], and Gary J. Melnick[7]

[1] National Astronomical Observatories, Chinese Academy of Sciences, Beijing 100101, China; dili@nao.cas.cn
[2] University of Chinese Academy of Sciences, Beijing 100049, China; jingwen@nao.cas.cn
[3] Research Center for Astronomical Computing, Zhejiang Laboratory, Hangzhou 311100, Zhejiang Laboratory, Hangzhou 311100, China
[4] Jet Propulsion Laboratory, California Institute of Technology, Pasadena, CA 91109, USA
[5] Institute for Frontiers in Astronomy and Astrophysics, Beijing Normal University, Beijing 102206, China
[6] KOSMA, I. Physik. Institut, Universität zu Köln, Zülpicher Str. 77, 50937 Köln, Germany
[7] Center for Astrophysics | Harvard & Smithsonian, 60 Garden Street, MS 66, Cambridge, MA 02138, USA
Received 2024 March 8; revised 2024 April 18; accepted 2024 April 22; published 2024 June 10

Abstract

The Submillimeter Wave Astronomy Satellite (SWAS) was the first space telescope capable of high spectral resolution observations of terahertz spectral lines. We have investigated the integration ability of its two receivers and spectrometer during five and a half years of on-orbit operation. The C I, O_2, H_2O, and ^{13}CO spectra taken toward all observed Galactic sources were analyzed. The present results are based on spectra with a total integration time of up to 2.72×10^4 hr ($\simeq 10^8$ s). The noise in the spectra is generally consistent with that expected from the radiometer equation, without any sign of approaching a noise floor. This noise performance reflects the extremely stable performance of the passively cooled front end as well as other relevant components in the SWAS instrument throughout its mission lifetime.

Key words: telescopes – space vehicles: instruments – instrumentation: miscellaneous – ISM: lines and bands

1. Introduction

Signals from many key spectral transitions required for understanding star-forming regions can be severely affected by the Earth's atmosphere, which contains the broad H_2O vapor lines and O_2 absorption bands at terahertz (300–3000 GHz) frequencies. Observing outside the Earth's atmosphere from a spacecraft completely avoids the spectral blockage by water vapor and O_2 in the Earth's atmosphere. In the past thirty years, several long-term space observation programs have been successfully carried out at submillimeter wavelengths by Submillimeter Wave Astronomy Satellite (SWAS, Melnick et al. 2000), Odin (Nordh et al. 2003) and Herschel (Pilbratt et al. 2010). Together with space infrared observatories (IRAS, Neugebauer et al. 1984; ISO, Kessler et al. 1996; Planck, Villa et al. 2002; AKARI, Murakami et al. 2007; Spitzer, Werner et al. 2004; WISE, Wright et al. 2010), they have started covering the "unexplored windows" left by ground-based observations (Doyle et al. 2009).

Compared with ground-based observations, the harsh space environment, the weight and size limits for the payloads, the power limits for the on-board instruments and lack of maintenance and supply for most missions are significant challenges to the performance and lifetime of the instrument systems in space, especially for long-term missions. To ensure that those observatories can function correctly on orbit throughout the mission as designed, tests have been applied to the instruments assembled aboard before being launched (Tolls et al. 2004). In some cases, the instruments' in-flight performance was also analyzed (Tolls et al. 2004; Nordh et al. 2003; Frisk et al. 2003; Lundin & Silverlind 2006; Teyssier et al. 2010; Roelfsema et al. 2012).

For on-orbit submillimeter observatories, the actual long-term on-orbit noise performance of the receivers and the stability of the whole observation system determine the feasibility of high sensitivity observations and of the reliability of the obtained data. For astronomical monitoring observations covering a very long period of time (e.g., Benmahi et al. 2020) and observations with ultra-long total integration time, they are of even more importance.

Measurements of the on-orbit noise performance and stability of receivers have been performed, including those for Odin (24 hr by Pagani et al. 2003 and 55 hr by Larsson et al. 2007). For SWAS, good on–orbit radiometric performance has been confirmed for its receivers right after system integration in Melnick et al. (2000) (up to 80 hr) as well as through a deep integration toward a single position for up to 383.3 hr in Tolls et al. 2004).

In this paper, we present the on-orbit long-term noise performance of the receivers aboard SWAS through a

[8] Corresponding author.

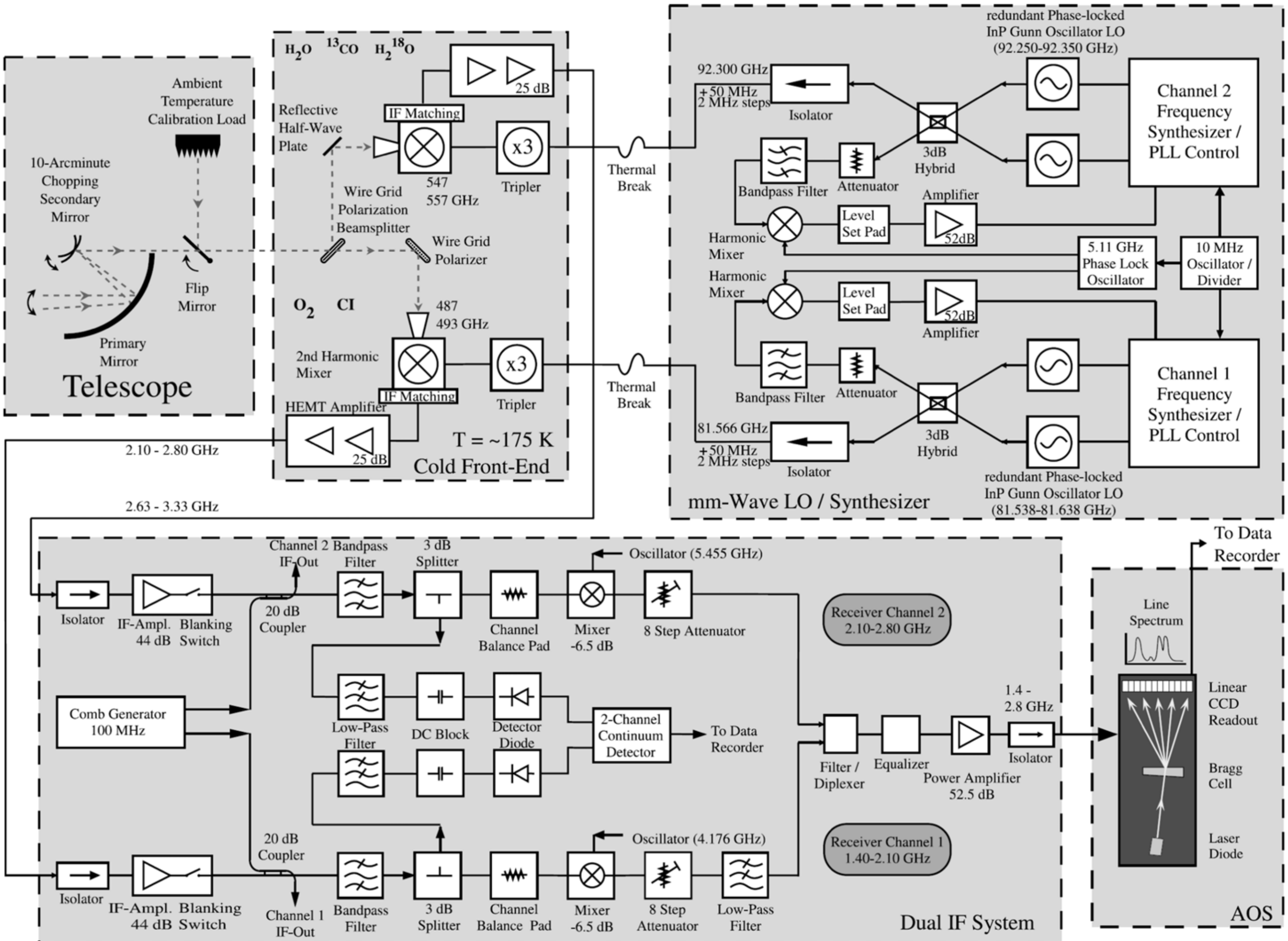

Figure 1. Block diagram of the SWAS instrument, from Tolls et al. (2004) (Figure 4). Receiver channel 1 (the lower channel in this diagram) covers the C I and O_2 line, while Receiver channel 2 (the upper channel in the diagram) covers the H_2O and ^{13}CO lines (also for the $H_2^{18}O$ line for a few sources).

comprehensive analysis of most of its archival data.[8] The results address the on-orbit long-term stability of the SWAS receivers as well as the complete spectroscopic system.

2. SWAS Instruments and Observations

SWAS had two double sideband (DSB) receivers (Receiver 1 and Receiver 2, respectively) to observe four molecular lines in four sidebands simultaneously. The Cold Front-End (CoFE) of the receivers was passively cooled. The SWAS spacecraft and instruments have been described in detail in Melnick et al. (2000) and Tolls et al. (2004). Figure 1 (from Tolls et al. 2004 (Figure 4)) shows the instruments.

The SWAS mission lasted 5.5 yr (Bergin & Melnick 2005). At every observed position, CI ($^3P_1 - {^3P_0}$, 492.161 GHz) and O_2 (3,3–1,2, 487.249 GHz) spectra were obtained by Receiver 1 while H_2O ($1_{10} - 1_{01}$, 556.936 GHz) and ^{13}CO ($J = 5$–4, 550.926 GHz) spectra (alternatively the $H_2^{18}O$ spectra ($1_{10} - 1_{01}$, 547.676 GHz, for a few sources) were obtained by Receiver 2 (Melnick et al. 2000). The on-board spectrometer resolved the signals from both sidebands of Receiver 1 and Receiver 2 simultaneously in separated bandpasses. Being in orbit around the Earth, observations toward the same celestial position were not carried out continuously, but intermittently for irregularly spaced intervals. Therefore, the quality of the combined spectra depends directly on the long-term performance and stability of the SWAS instrument.

The performance of the SWAS instrument was tested before the launch and in-flight (Tolls et al. 2004). The mixers, the frequency triplers, and the local oscillator did not degrade significantly during the first 1700 mission days (Tolls et al. 2004).

[8] http://irsa.ipac.caltech.edu/applications/SWAS/SWAS/list.html

Laser diode 1 in the acousto-optical spectrometer (AOS) was replaced by the redundant laser diode 2 nearly two years after launch (Tolls et al. 2004). The SWAS spacecraft's on-orbit pointing strategy helped to realize effective passive cooling of the cold front end components (frequency triplers to provide the local oscillator power at approximately half the input frequencies, second harmonic mixers and first IF amplifiers). The variation of the physical temperature of the receiver system is less than 0.2 K per hour and 2 K per days during nominal operation (Tolls et al. 2004).

The SWAS scans were averaged into a "combined" spectrum.[9] Most of the SWAS "combined" spectra have an on-source integration time of 360 s and a total integration time of 720 s. For the sake of simplicity, we refer to them all as "the 720 s spectra" with total integration time of 720 s (on+off). Starting from this, we investigate the actual spectral baseline noise performance corresponding to longer total integration time obtained via the intermittent long-term on-orbit sampling.

Since the spectra are the outputs of the SWAS observation system, the observed noise and spectral baseline performance will reflect not only the performance of the receivers, but also the performance of the whole on-orbit observation system including IF chain, second down converters, and AOS.

3. Data Reduction

The data of all the 386 Galactic sources observed by SWAS were downloaded from the SWAS spectrum service of the NASA/IPAC infrared science archive.

To perform our analysis, the data were reduced in the following steps. First, for the observations toward the same position, the 720 s spectra of the same line were combined. Next, the antenna temperatures of these combined spectra were corrected for the SWAS main-beam efficiency of 0.90. After these two steps, for every combined spectrum, a 50 km s^{-1} wide "clean" interval without spectral feature and/or spurious signals in the baseline was selected.[10]

Next, all the "clean" intervals were aligned to the same velocity interval, 0–50 km s^{-1}. Subsequently, a linear baseline was subtracted from this interval. We call these "clean-interval-aligned" spectra toward every observed position the "treated" spectra. We obtained the "treated" spectra for C I, O_2, H_2O and ^{13}CO lines. We next generated the composite average spectra by adding all the "treated" spectra while aligning them in velocity. Subsequently, the baseline noise performance of composite average spectra was analyzed as a function of total integration time.

[9] These "combined" spectra were generated through the pipeline described in Wang et al. (1996).

[10] In order to avoid the effect of spurious lines and astronomical features on the baseline noise performance to the maximum extent possible, we selected the interval with minimum rms noise as the "clean" interval. We obtained the intervals using a Nyquist sampling with a step length of 50 km s^{-1} for the zero-value-ends-off spectrum interval.

In our analysis in this paper, for individual "treated" spectra and the composite average spectra, the root mean square (rms) noise per channel values were calculated using the channels in the "clean" interval. Considering the significant variation in integration time among different observed positions, we adopted the mode of weighting by integration time[11] when generating both the "treated" spectra and the composite average spectra using the GILDAS CLASS software.

4. Results and Analysis

We adopted all of the C I, O_2, H_2O, and ^{13}CO spectra of 385 out of a total of 386 sources to analyze the baseline noise performance with ultra–long total integration time. Below we present the results and analysis.

4.1. Noise of the Composite Average Spectra

According to the radiometer equation (e.g., Equation A2 in Goldsmith et al. 2002), for SWAS spectra we have

$$\sigma = \frac{2T_{\rm ssb}}{\sqrt{\Delta f t_{\rm int}}}, \tag{1}$$

where σ is the rms noise per channel in K and $T_{\rm ssb}$ is the single sideband system noise temperature in K. Δf is the frequency resolution in Hz, taken as 2.18 MHz (i.e., the fluctuation bandwidth discussed in Tolls et al. (2004), considering the non-independent adjacent channels in the AOS). $t_{\rm int}$ is the total integration time (on-source + off-source) in seconds.[12]

In our calculation of the theoretical rms noise, $T_{\rm ssb}$ was taken as twice the double sideband system noise temperature $T_{\rm dsb}$, i.e., the system temperature $T_{\rm sys}$ recorded in the SWAS data.[13] The total integration time $t_{\rm int}$ we adopted is twice the integration time value (the on-source time) recorded in the SWAS spectral data.

Figure 2 shows the log–log diagram of the rms noise per channel versus total integration time (on+off) for the composite average spectra of C I, O_2 (sampled by Receiver 1, upper panel), H_2O, and ^{13}CO (sampled by Receiver 2, lower panel). The "treated" spectra of every observed position of 385 in all 386 interstellar sources observed by SWAS during its long-term mission were accumulated.

The total integration time increases, reaching an overall total integration time of 2.72 $\times 10^4$ hr (9.80 $\times 10^7$ s for C I/O_2 lines) or 2.47 $\times 10^4$ hr (8.90 $\times 10^7$ s for H_2O/^{13}CO lines[14]). For

[11] see www.iram.fr/IRAMFR/GILDAS/doc/pdf/class.pdf.

[12] For SWAS, the equal sampling time toward the observed and reference position in its position switching observational mode induces a factor of 2 into the radiometer equation.

[13] With a sideband gain ratio of unity assumed (as in Goldsmith et al. 2002) for both receivers. This is reasonable given the low IF frequency compared to the RF frequency and has been confirmed by both prelaunch (Tolls et al. 2004) and on-orbit (Melnick et al. 2000; Neufeld et al. 2000) tests.

[14] The $H_2^{18}O$ spectra are not included as this line was observed toward relatively few sources.

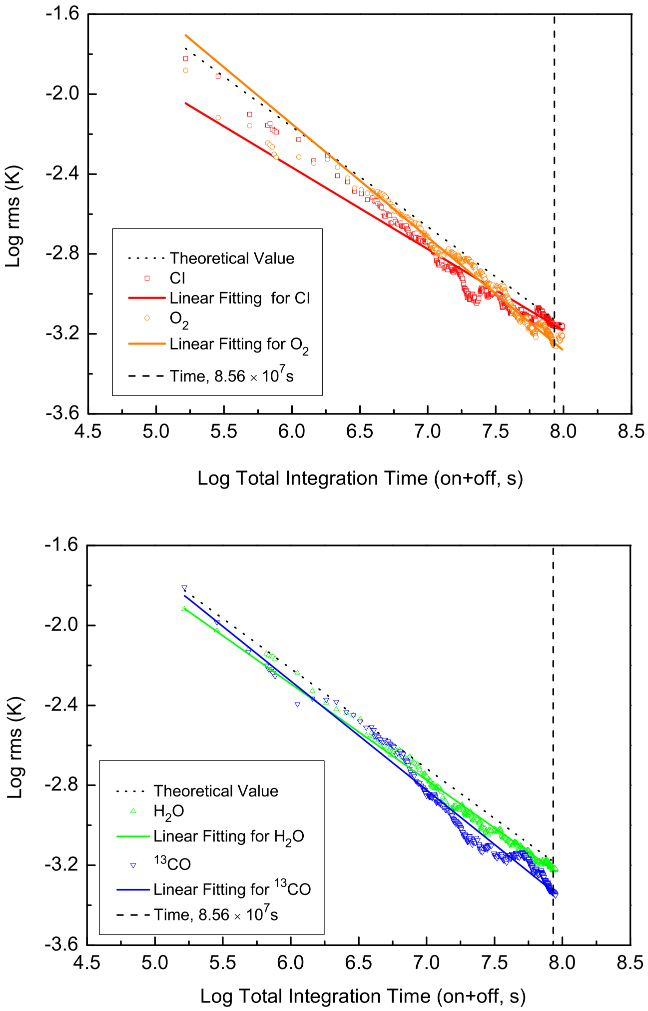

Figure 2. Log–log rms noise per channel vs. total integration time (on+off) for the four lines observed by SWAS Receiver 1 (upper panel) and 2 (lower panel). The red open squares, orange circles, green open triangles and blue open inverted triangles represent the composite average spectra of C I , O_2, H_2O and ^{13}CO lines, respectively. The black dotted lines indicate the corresponding theoretical rms values of noise. The black dashed vertical lines correspond to a total integration time of 2.38×10^4 hr ($\simeq 1\times 10^8$ s). The red, orange, green and blue solid straight lines represent the results of linear fits to the rms noise per channel—total integration time relation for the C I, O_2, H_2O and ^{13}CO composite average spectra, respectively. The overall rms noise values and the parameters of the fitting results are listed in Table 1.

the four primary lines, the "treated" spectra of most positions are of the same total integration time and were accumulated in the same order until an overall total integration time of $2.38\ \times 10^4$ hr is reached. Then the "treated" spectra with different total integration time for C I /O_2 and H_2O/^{13}CO for the same position were accumulated in the same order.

In Figure 2, the rms noise of the composite average spectra for all four lines decreases with increasing total integration time with values of rms noise per channel for the composite average spectra close to the theoretical values (the black dotted lines; see Appendix for discussion of the lower-than-theoretical actual rms noise). The red, orange, green and blue solid lines in Figure 2 presents the linear fit results for the baseline noise per channel versus total integration time relation for C I, O_2, H_2O and ^{13}CO spectra, respectively. The overall rms noise values and the parameters of the fitted results are listed in Table 1.

Table 1
Overall rms Noise and Results of Linear Fitting for the rms Noise per Channel vs. Total Integration Time Relations Shown in Figure 2

Line	Overall rms (K)	Slope	Intercept	Adjusted R-square
C I	6.90×10^{-4}	-0.41 ± 0.001	0.087 ± 0.009	0.94
O_2	6.17×10^{-4}	-0.57 ± 0.001	1.25 ± 0.010	0.97
H_2O	6.04×10^{-4}	-0.48 ± 0.0006	0.59 ± 0.005	0.99
^{13}CO	4.46×10^{-4}	-0.55 ± 0.001	0.99 ± 0.009	0.97

4.2. *"Jump Points"*

We note that there are jump points where there are sudden rises in the rms value. The spectra that cause the jump points are noisier,[15] e.g., exhibiting sawtooth-like baseline ripple. Such abnormal ripples can appear in one or both sidebands. We repeated the analysis excluding these abnormal "treated" spectra for both sidebands (Figure 3 and Table 2). The resulting final rms noise decreases to even lower values and the overall slopes of linear fitting results decrease for both sidebands. The overall adjusted R-square values change little, remaining close to 1 (see Table 2).

5. Conclusions

In this paper, we have presented a comprehensive analysis of the long term (5.5 yr mission time) on-orbit noise performance of the SWAS instrument for high-resolution observations of spectral lines in the 485 to 560 GHz frequency range.

1. We have included C I, O_2, H_2O, and ^{13}CO spectra toward 385 Galactic sources. The noise level toward each position is close to that theoretically expected (see Appendix) and previously measured (e.g., Goldsmith et al. 2000, 2002).

2. We have combined a total of 2.72×10^4 hr of observations by Receiver 1 (for C I and O_2 lines) and 2.49×10^4 hr by Receiver 2 (for H_2O and ^{13}CO lines). These amount to more than 30 times the total integration time included in the previous analysis by Tolls et al. (2004).

3. The rms noise in the composite average spectra of the C I /O_2 lines observed by Receiver 1 and H_2O/^{13}CO observed by Receiver 2 all follow the radiometer equation, with σ

[15] And their relatively long total integration time brings them relatively high weighting when generating the composite average spectra.

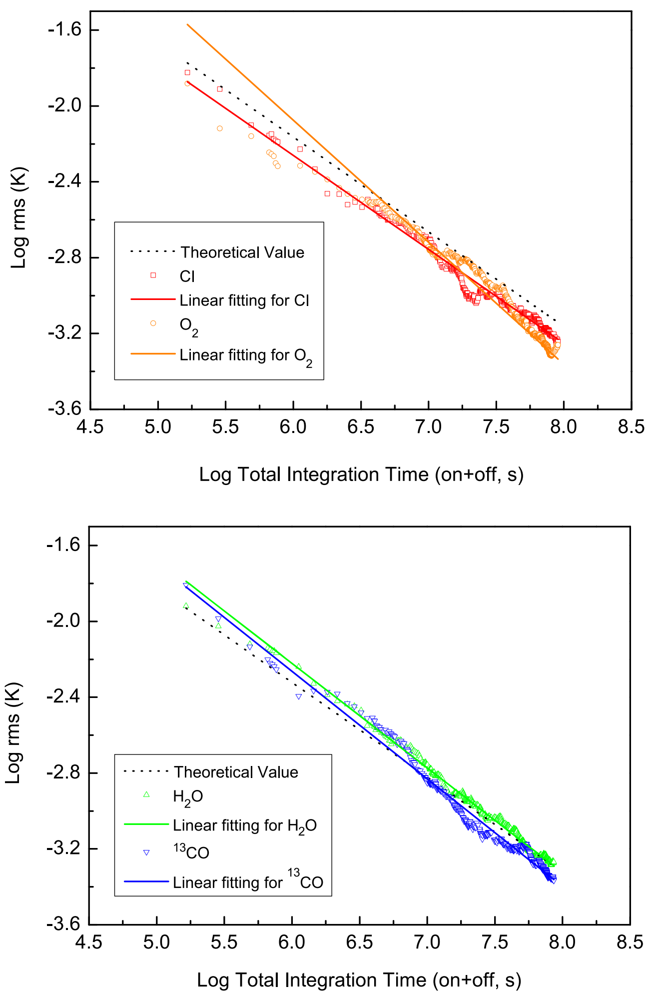

Figure 3. Log–log rms noise per channel vs. total integration time (on+off) for the four lines observed by SWAS Receiver 1 (upper panel) and 2 (lower panel), with eight (for Receiver 1) and six (for Receiver 2) abnormal "treated" spectra excluded, respectively. The red open squares, orange circles, green open triangles and blue open inverted triangles represent the composite average spectra of C I, O_2, H_2O and ^{13}CO lines, respectively. The black dotted lines represent the corresponding theoretical rms noise values. The red, orange, green and blue solid straight lines represent the linear fitting results for the log–log rms noise per channel vs. total integration time relation of the C I, O_2, H_2O and ^{13}CO composite average spectra, respectively. The overall rms noise values and the parameters of the fitting results are listed in Table 2.

deceasing roughly as $t^{-0.5}$, without reaching any noise floor for a total integration time of more than 2×10^4 hr ($\simeq 10^8$ s).

Our results show that the integration capability of the passively cooled Schottky mixer heterodyne front end of SWAS was outstanding. This demonstrates the great potential of such radiometer systems for future long-term missions if proper environmental conditions, including but not only good thermal stability, can be maintained. In the SWAS case, the effective passive cooling of the CoFE is realized generally by being usually in eclipsed orbits and at a thermal-safe attitude (Tolls et al. 2004).

Table 2
Overall rms Noise and Results of Linear Fitting for the rms Noise per Channel vs. Total Integration Time Relations Shown in Figure 3

Line	Overall rms (K)	Slope	Intercept	Adjusted R-square
C I	5.70×10^{-4}	-0.50 ± 0.0009	0.71 ± 0.007	0.98
O_2	5.49×10^{-4}	-0.64 ± 0.001	1.79 ± 0.011	0.97
H_2O	5.37×10^{-4}	-0.55 ± 0.0006	1.09 ± 0.005	0.99
^{13}CO	4.31×10^{-4}	-0.57 ± 0.0009	1.14 ± 0.007	0.98

Acknowledgments

This work is supported by the National Natural Science Foundation of China (NSFC; Grant Nos. 11988101 and 12041302), the International Partnership Program of the Chinese Academy of Sciences (grant No. 114A11KYSB20210010) and National Key R&D Program of China No. 2023YFA1608004. D.L. is a New Cornerstone Investigator of the New Cornerstone Science Laboratory. This research utilized the NASA/IPAC Infrared Science Archive, which is funded by the National Aeronautics and Space Administration and operated by the California Institute of Technology. This research was carried out in part at the Jet Propulsion Laboratory, which is operated by the California Institute of Technology under a contract with the National Aeronautics and Space Administration (80NM0018D0004). We acknowledge the block diagram of the SWAS instrument taken from Tolls et al. (2004). We would like to thank Lei Qian and Xinxin Zhang for their help and the discussion. We would like to thank the anonymous referee and the scientific editor for the valuable advice for our paper and for helping us improve our work.

Appendix
Additional Information on Noise in SWAS "treated" Spectra

The actual rms noise per channel in the 50 km s^{-1} "clean" intervals of the "treated" spectra and the corresponding theoretical rms noise of every SWAS observed position involved in our analysis are both calculated for the C I, O_2, H_2O and ^{13}CO lines. Figure A1 shows the actual rms/theoretical rms ratio (denoted $R_{\mathrm{actu/theo}}$) plotted against the logarithm of the total integration time for these "treated" spectra. For all four lines, the "treated" spectra form two obvious groups divided by a total integration time of $10^{3.1}$ s (1259 s). The statistics of these two groups are given in Table A1.

Most of the actual rms noise values of the "treated" spectra are lower than those expected theoretically (from the radiometer equation; Equation (1).) This may be the combined result of SWAS hardware, LO controlling software and data reduction software. The SWAS AOS has a complex frequency

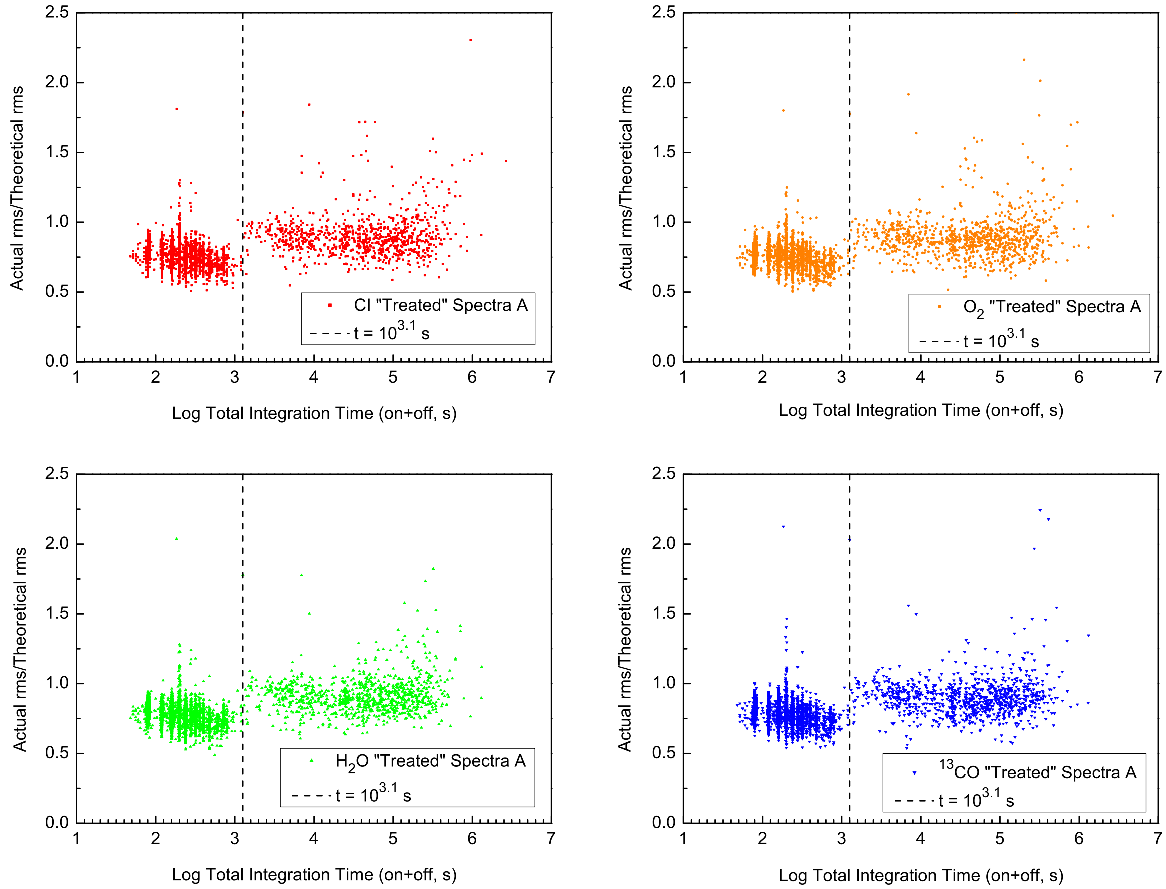

Figure A1. $R_{\mathrm{actu/theo}}$ of the 50 km s^{-1} "clean" intervals of the "treated" spectra of every observed position for C I (red solid squares, upper left panel), O_2 (orange solid circles, upper right panel), H_2O (green solid triangles, lower left panel) and ^{13}CO (blue solid inverted triangles, lower right panel) lines against the corresponding total integration time (on+off). The black dashed vertical lines represent a total integration time of $10^{3.1}$ s (1259 s). The arithmetic mean and standard deviation of the actual rms/theoretical rms ratio ($R_{\mathrm{actu/theo}}$) of each group are listed in Table A1.

Table A1
Statistics of $R_{\mathrm{actu/theo}}$ in Figure A1

Line	AM and SD[a] of $R_{\mathrm{actu/theo}}$	Observed Number of Positions[b]	Sum of $t_{\mathrm{on+off}}$, on Percentage[c]	AM and SD[a] of $R_{\mathrm{actu/theo}}$	Observed Number of Positions[b]	Sum of $t_{\mathrm{on+off}}$, on Percentage[c]
	(For "treated" spectra with $t_{\mathrm{on+off}} \leqslant 10^{3.1}$ s)[d]			(For "treated" spectra with $t_{\mathrm{on+off}} > 10^{3.1}$ s)[d]		
C I	0.76 ± 0.07	5983	1.2%	0.90 ± 0.16	963	98.8%
O_2	0.76 ± 0.07			0.90 ± 0.17		
H_2O	0.78 ± 0.07	5983	1.4%	0.92 ± 0.14	960	98.6%
^{13}CO	0.78 ± 0.07			0.90 ± 0.15		

Notes.
[a] The arithmetic mean and standard deviation of $R_{\mathrm{actu/theo}}$.
[b] The number of observed positions, i.e., the number of "treated" spectra.
[c] The percentage of the sum of the total integration time $t_{\mathrm{on+off}}$ of these "treated" spectra in the overall total integration time.
[d] See Figure A1.

Table A2
T_{ssb} and Theoretical/Actual rms Noise per Channel of the "treated" Spectra of 38 SWAS Sources

Source	Total Integration time t_{int} (on+off, s)	T_{ssb} of "treated" Spectra (K)		Theoretical rms Noise of "treated" Spectra (K)		$R_{actu/theo}$			
		C I / O_2	H_2O / ^{13}CO	C I / O_2	H_2O / ^{13}CO	C I	O_2	H_2O	^{13}CO
(1)	(2)	(3)	(4)	(5)	(6)	(7)	(8)	(9)	(10)
G10.47+0.03	6.13×10^4	5.09×10^3	4.55×10^3	2.78×10^{-2}	2.48×10^{-2}	0.671	1.000	0.703	0.871
G10.47+45	1.09×10^5	5.06×10^3	4.59×10^3	2.07×10^{-2}	1.87×10^{-2}	0.978	0.848	0.943	0.903
G10.6-0.4	2.21×10^5	5.08×10^3	4.52×10^3	1.46×10^{-2}	1.29×10^{-2}	1.010	0.837	1.070	0.957
G10.6-0.4-NO1	4.59×10^4	5.04×10^3	4.53×10^3	3.18×10^{-2}	2.85×10^{-2}	0.952	0.881	0.808	1.070
G111.6+0.37	1.36×10^4	5.11×10^3	4.56×10^3	5.93×10^{-2}	5.28×10^{-2}	0.834	0.859	0.864	0.940
G12.21-0.01	7.97×10^4	5.09×10^3	4.56×10^3	2.44×10^{-2}	2.18×10^{-2}	0.958	0.865	0.947	0.882
G19.37-0.03	2.99×10^4	5.09×10^3	4.58×10^3	3.98×10^{-2}	3.57×10^{-2}	0.799	0.725	0.831	0.960
G19.40-0.01	1.30×10^5	5.01×10^3	4.53×10^3	1.88×10^{-2}	1.70×10^{-2}	0.919	0.876	0.992	0.791
G23.95+0.15	1.39×10^5	5.02×10^3	4.59×10^3	1.82×10^{-2}	1.66×10^{-2}	0.892	1.020	0.886	0.858
G261.6-2.1	1.53×10^5	5.02×10^3	4.51×10^3	1.74×10^{-2}	1.56×10^{-2}	0.864	0.841	0.880	1.010
G268.4-0.9	4.78×10^5	5.02×10^3	4.52×10^3	9.81×10^{-3}	8.80×10^{-3}	0.662	1.180	0.846	0.703
G269.2-1.1	8.86×10^4	5.10×10^3	4.55×10^3	2.32×10^{-2}	2.06×10^{-2}	0.880	0.849	0.915	1.010
G269.2-1.1+30	5.04×10^5	5.12×10^3	4.55×10^3	9.77×10^{-3}	8.63×10^{-3}	1.230	0.956	0.906	0.898
G269.5-1.47	2.72×10^4	5.02×10^3	4.51×10^3	4.12×10^{-2}	3.68×10^{-2}	0.838	0.903	0.779	0.927
G285.3-0.1	2.56×10^5	5.00×10^3	4.50×10^3	1.34×10^{-2}	1.20×10^{-2}	1.070	0.812	0.759	0.906
G286.2+0.2	6.51×10^3	5.14×10^3	4.53×10^3	8.62×10^{-2}	7.57×10^{-2}	0.964	0.882	0.867	0.874
G293.8-0.74	1.50×10^4	5.10×10^3	4.54×10^3	5.64×10^{-2}	5.00×10^{-2}	0.926	0.767	0.822	0.889
G294.0-0.90	1.54×10^4	5.10×10^3	4.55×10^3	5.56×10^{-2}	4.94×10^{-2}	0.911	0.955	0.946	0.989
G294.5-1.6	1.37×10^5	5.03×10^3	4.49×10^3	1.84×10^{-2}	1.64×10^{-2}	0.780	0.642	0.824	0.845
G295.0-1.7	2.80×10^5	5.10×10^3	4.52×10^3	1.30×10^{-2}	1.15×10^{-2}	0.991	0.821	0.899	0.915
G302.0-0.06	2.40×10^4	5.12×10^3	4.57×10^3	4.47×10^{-2}	3.98×10^{-2}	0.789	0.844	0.880	0.760
G31.41+0.31	9.94×10^4	5.03×10^3	4.61×10^3	2.16×10^{-2}	1.97×10^{-2}	0.854	0.841	0.819	0.848
G312.1+0.31	2.70×10^4	5.05×10^3	4.48×10^3	4.16×10^{-2}	3.67×10^{-2}	0.841	0.953	0.881	0.816
G32.96+0.28	3.05×10^4	5.07×10^3	4.54×10^3	3.93×10^{-2}	3.51×10^{-2}	0.963	0.763	0.886	0.904
G322.2+0.6	3.48×10^4	5.03×10^3	4.45×10^3	3.65×10^{-2}	3.22×10^{-2}	0.828	0.825	0.966	0.881
G324.9-0.57	1.15×10^4	5.10×10^3	4.51×10^3	6.44×10^{-2}	5.67×10^{-2}	0.701	0.936	0.790	1.050
G327.3-0.5	8.05×10^4	5.11×10^3	4.52×10^3	2.44×10^{-2}	2.15×10^{-2}	0.894	0.649	0.888	0.742
G328.8+0.63	1.34×10^4	5.08×10^3	4.47×10^3	5.95×10^{-2}	5.21×10^{-2}	0.910	0.707	0.925	0.937
G329.3+0.15	1.19×10^4	5.08×10^3	4.46×10^3	6.30×10^{-2}	5.51×10^{-2}	0.915	0.884	0.935	0.970
G333.1-0.4	2.77×10^5	5.15×10^3	4.53×10^3	1.32×10^{-2}	1.16×10^{-2}	0.856	0.784	1.020	1.100
G34.3+0.1	3.12×10^5	5.04×10^3	4.53×10^3	1.22×10^{-2}	1.09×10^{-2}	0.892	0.969	1.050	0.856
G34.3+0.1+15	1.48×10^5	5.04×10^3	4.56×10^3	1.77×10^{-2}	1.60×10^{-2}	0.870	0.950	0.991	0.992
G45.07+0.13	5.22×10^3	5.10×10^3	4.55×10^3	9.54×10^{-2}	8.48×10^{-2}	0.810	0.905	1.000	1.000
G48.61+0.02	3.12×10^4	5.08×10^3	4.57×10^3	3.89×10^{-2}	3.48×10^{-2}	0.913	0.871	1.090	0.878
G5.89-0.39	4.33×10^3	5.08×10^3	4.55×10^3	1.04×10^{-1}	9.32×10^{-2}	0.981	0.879	0.929	0.962
G59.78+0.06	4.67×10^4	5.15×10^3	4.58×10^3	3.22×10^{-2}	2.86×10^{-2}	0.935	0.789	0.736	0.982
G60.89-0.13	1.25×10^4	5.06×10^3	4.53×10^3	6.11×10^{-2}	5.46×10^{-2}	0.962	0.788	0.849	1.020
G80.87+0.42-NO1	1.38×10^5	5.01×10^3	4.48×10^3	1.82×10^{-2}	1.62×10^{-2}	0.846	0.677	0.959	0.826
Average	⋯	5.07×10^3	4.53×10^3	3.65×10^{-2}	3.25×10^{-2}	0.892	0.856	0.897	0.914
Std.Dev.	⋯	41.1	35.8	2.40×10^{-2}	2.12×10^{-2}	0.104	0.104	0.0891	0.0881
Minimum	4.33×10^3	5.00×10^3	4.46×10^3	9.77×10^{-3}	8.63×10^{-3}	0.662	0.642	0.703	0.703
Maximum	5.04×10^5	5.15×10^3	4.61×10^3	1.04×10^{-1}	9.32×10^{-2}	1.23	1.18	1.09	1.10

response. The fluctuation bandwidth (noise bandwidth) we adopted to derive the theoretical noise values according to Equation (1) was derived in the prelaunch tests in the laboratory and there was no Doppler effect or spectra frequency correction (shifting) when calculating the noise bandwidth (Tolls et al. 2004). In the on–orbit observing, the changing Doppler effect, which cannot be eliminated in real–time, degrades the AOS spectral resolution (Frerick et al. 1999). In the offline data calibration and reduction to correct the remaining Doppler effect after observation, frequency shifts were performed on the 2 s scans by multiples of the AOS frequency pixel spacing and then the scans were reduced to the co-adds (e.g., the 720 s spectra in this paper). This process further degrades (although by a small amount) the spectral resolution (Tolls et al. 2004). As a further averaging operation, the combining of the co-adds using the CLASS software may further lower the spectra resolution. All these factors increase the effective noise bandwidth of a given channel. Although there is no simple quantitative correction, the results presented here give empirical values for the increase in the effective noise bandwidth which is a factor of 1.2 to 1.7,[16] according to the average $R_{\mathrm{actu/theo}}$ values of 0.76–0.92 in Table A1.

For both groups, $R_{\mathrm{actu/theo}}$ and corresponding standard deviations are highly consistent for the lines observed by the same receivers. Within each group, the $R_{\mathrm{actu/theo}}$ values show no significant trends as a function of increasing total integration time. The group with $t_{\mathrm{on+off}} \leqslant 10^{3.1}$ s[17] has lower average values of $R_{\mathrm{actu/theo}}$ and corresponding standard deviations.

The "treated" spectra with $t_{\mathrm{on+off}} \leqslant 10^{3.1}$ s dominate the number of positions observed. For this group, the corresponding average $1/R_{\mathrm{actu/theo}}$ is 1.3 for the four lines analyzed. It is close to those reported previously for SWAS observations ($1/R_{\mathrm{actu/theo}} = 1.5$ (with a somewhat smaller AOS noise bandwidth) in Goldsmith et al. (2000); $1/R_{\mathrm{actu/theo}} = 1.38$, in Goldsmith et al. 2002). The "treated" spectra with $t_{\mathrm{on+off}} > 10^{3.1}$ s are the dominant contribution to the overall integration time. For this group, the corresponding average $1/R_{\mathrm{actu/theo}}$ is 1.1 for the four lines analyzed. Taking both groups into consideration, we adopt 1.2 as the average $1/R_{\mathrm{actu/theo}}$ value, i.e., the average ratio of theoretical rms noise to actual rms noise obtained in our analysis of the SWAS system.

As a detailed example of the latter group, parameters of the "treated" spectra (described in Section 3) of 38 SWAS sources (∼10% of the total of all sources we analyzed) with only one observed position are listed in Table A2. The upper and lower sidebands of the same receiver share the same single sideband noise temperature and the same theoretical rms value. The parameters listed are the source (column (1)), the total integration time (column (2)), the single sideband noise temperature (T_{ssb}, columns (3)–(4)), the theoretical rms noise per channel (columns (5)–(6)), and the ratio of the calculated actual rms noise per channel in the "clean" interval in the baseline of every "treated" spectrum to the corresponding theoretical rms value ($R_{\mathrm{actu/theo}}$, columns (7)–(10)). The average values of the ratio of actual (measured) noise to theoretical (radiometer equation) noise, $R_{\mathrm{actu/theo}}$, are 0.89 for C I, 0.86 for O_2, 0.90 for H_2O and 0.91 for ^{13}CO line. The standard deviations of $R_{\mathrm{actu/theo}}$ are 0.104 for C I, 0.104 for O_2, 0.089 for H_2O, and 0.088 for ^{13}CO, respectively. These values are consistent with those of the $t_{\mathrm{on+off}} > 10^{3.1}$ s group presented in Figure A1 and Table A1.

[16] For the "clean" interval in the baseline of the "treated" spectra (also the average spectra toward every observed position).

[17] These "treated" spectra are mostly in the large area mapping observations toward three sources: Rho Oph A, OMC-1 and M17SW.

ORCID iDs

Bing-Ru Wang https://orcid.org/0009-0001-8411-5096
Di Li https://orcid.org/0000-0003-3010-7661
Paul F. Goldsmith https://orcid.org/0000-0002-6622-8396
Jingwen Wu https://orcid.org/0000-0001-7808-3756
Chao-Wei Tsai https://orcid.org/0000-0002-9390-9672
Gary J. Melnick https://orcid.org/0000-0002-6025-0680

References

Benmahi, B., Cavalié, T., Dobrijevic, M., et al. 2020, A&A, 641, A140
Bergin, E. A., & Melnick, G. J. 2005, Astrochemistry: Recent Successes and Current Challenges Proc. IAU Symp. No. 231 (Cambridge: Cambridge Univ. Press), 309
Doyle, D., Pilbratt, G., & Tauber, J. 2009, IEEEP, 97, 1403
Frerick, J., Klumb, M., Schieder, R., et al. 1999, Proc. SPIE, 3759, 170
Frisk, U., Hagström, M., Ala-Laurinaho, J., et al. 2003, A&A, 402, L27
Goldsmith, P. F., Melnick, G. J., Bergin, E. A., et al. 2000, ApJ, 539, L123
Goldsmith, P. F., Li, D., Bergin, E. A., et al. 2002, ApJ, 576, 814
Kessler, M. F., Steinz, J. A., Anderegg, M. E., et al. 1996, A&A, 315, L27
Larsson, B., Liseau, R., Pagani, L., et al. 2007, A&A, 466, 999
Lundin, S., & Silverlind, S.-O. 2006, AcAau, 59, 503
Melnick, G. J., Stauffer, J. R., Ashby, M. L. N., et al. 2000, ApJ, 539, L77
Murakami, H., Baba, H., Barthel, P., et al. 2007, PASJ, 59, S369
Neufeld, D. A., Snell, R. L., Ashby, M. L. N., et al. 2000, ApJ, 539, L107
Neugebauer, G., Habing, H. J., Van Duinen, R., et al. 1984, ApJ, 278, L1
Nordh, H. L., von Schéele, F., Frisk, U., et al. 2003, A&A, 402, L21
Pagani, L., Olofsson, A. O. H., Bergman, P., et al. 2003, A&A, 402, L77
Pilbratt, G. L., Riedinger, J. R., Passvogel, T., et al. 2010, A&A, 518, L1
Roelfsema, P. R., Helmich, F. P., Teyssier, D., et al. 2012, A&A, 537, A17
Teyssier, D., Risacher, C., Dieleman, P., et al. 2010, 21st Int. Symp. on Space Terahertz Technology (Oxford: National Radio Astronomy Observatory (NRAO)), 40
Tolls, V., Melnick, G. J., Ashby, M. L. N., et al. 2004, ApJS, 152, 137
Villa, F., Bersanelli, M., Burigana, C., et al. 2002, AIP Conf. Proc., 616 (Melville, NY: AIP) 224
Wang, Z., Ashby, M. L. N., Plume, R., et al. 1996, BAAS, 28, 987
Werner, M. W., Reollig, T. L., & Low, F. J. 2004, ApJS, 154, 1
Wright, E. J., Eisenhardt, P. R. M., Mainzer, A. K., et al. 2010, AJ, 140, 1868